

INORGANIC CHEMISTRY

FRONTIERS

Accepted Manuscript



This article can be cited before page numbers have been issued, to do this please use: P. Salcedo-Abraira, Y. Pérez, C. García-Abad, N. Guillou, P. Horcajada and T. Devic, *Inorg. Chem. Front.*, 2026, DOI: 10.1039/D5QI02257F.



This is an Accepted Manuscript, which has been through the Royal Society of Chemistry peer review process and has been accepted for publication.

Accepted Manuscripts are published online shortly after acceptance, before technical editing, formatting and proof reading. Using this free service, authors can make their results available to the community, in citable form, before we publish the edited article. We will replace this Accepted Manuscript with the edited and formatted Advance Article as soon as it is available.

You can find more information about Accepted Manuscripts in the [Information for Authors](#).

Please note that technical editing may introduce minor changes to the text and/or graphics, which may alter content. The journal's standard [Terms & Conditions](#) and the [Ethical guidelines](#) still apply. In no event shall the Royal Society of Chemistry be held responsible for any errors or omissions in this Accepted Manuscript or any consequences arising from the use of any information it contains.

This work is licensed under CC BY 4.0. To view a copy of this license, visit <https://creativecommons.org/licenses/by/4.0/>

View Article Online
DOI: 10.1039/D5QI02257F

Vanadium thiocarboxylate Metal-Organic Frameworks as efficient photocatalysts for photooxidative desulfurization

Pablo Salcedo-Abraira^{*1,2}, Yolanda Pérez^{*3,4}, Clara García-Abad³, Nathalie Guillou⁵, Patricia Horcajada³, Thomas Devic^{*2}

¹ Department of Inorganic Chemistry, University of Granada, Avda. Fuente nueva s/n, 18071 Granada, Spain. E-mail: psalcedo@ugr.es

² Nantes Université, CNRS, Institut des Matériaux de Nantes Jean Rouxel, IMN, F-44000 Nantes, France. E-mail: thomas.devic@cnrs-imn.fr

³ IMDEA Energy Institute, Advanced Porous Materials Unit (APMU), Avda. Ramón de la Sagra 3, E-28935 Móstoles, Madrid, Spain. E-mail: yolanda.cortes@urjc.es

⁴ COMET-NANO group, Departamento de Biología y Geología, Física y Química Inorgánica, ESCET, Universidad Rey Juan Carlos, C/ Tulipán s/n, 28933, Móstoles, Madrid, Spain

⁵ Institut Lavoisier de Versailles, UMR CNRS 8180, Université de Versailles St-Quentin en Yvelines, Université Paris Saclay, 78035 Versailles, France.

Abstract

Air pollution causes the premature death of *ca.* 7 million people each year, with SO_x gases being among the most harmful contaminants. Reducing the sulfur content in liquid fossil fuels is crucial to overcoming this health and environmental issue. Among the different available technologies, photooxidative desulfurization (PODS) stand out as one of the most promising methods, since it only requires sunlight to drive the reaction. Metal-Organic Frameworks (MOFs), with exceptional porosity and chemical diversity, have emerged as potential adsorbents and photocatalysts for the removal of sulfur-containing compounds from fuels. In this work, the reactivity of the ligand 2,5-disulfhydrylbenzene-1,4-dicarboxylic acid (H₄DSBDC) with different V salts was evaluated to prepare new photocatalytically active Metal-Organic Frameworks. Two new compounds, labeled as (DMA)KV^{IV}O(DSBDC) and MIL-47(V^{III})-(SCH₃)₂, were successfully synthesized via solvothermal methods. X-Ray diffraction structure analysis revealed that the second solid relies exclusively on V-O bonds, whereas both V-O and V-S bonds are found in the first one. Both MOFs are stable in suspension and absorb light in the visible region, prompting their evaluation as photocatalysts for visible-light-driven reactions. For the first time, V-based Metal-Organic Frameworks are proposed for the photooxidative desulfurization reaction. Among them, MIL-47(V)-(SCH₃)₂ demonstrated superior performance, achieving a desulfurization efficiency of 73%, which was maintained for at least 4 consecutive cycles.

Introduction

According to the World Health Organization (WHO), approximately 7 million premature deaths are caused each year due to exposure to air pollutions,¹ recommending air quality levels for 6 key contaminants: nitrogen dioxide (NO₂), sulfur dioxide (SO₂), carbon monoxide (CO), ozone (O₃) and particulate matter (PM). In this context, the combustion of sulfur-containing compounds in conventional fossil fuels (*e.g.*, gasoline and diesel) releases harmful sulfur oxides (SO_x) into the atmosphere, which



react with water forming acid rain. Therefore, reducing the sulfur content in liquid fuels is urgently required to mitigate serious environmental and health issues caused by SO₂ emissions,² and to comply with demanding regulations (*i.e.* 10-15 ppm of sulfur)³ aimed at achieving ultra-low sulfur fuel standards. To date, various methods have been developed to remove sulfur from fuels, including adsorptive desulfurization (ADS), biodesulfurization (BDS), oxidative desulfurization (ODS), extractive desulfurization (EDS) and hydrodesulfurization (HDS).⁴ Among them, HDS is the most widely used technology. However, it requires harsh operating conditions (*i.e.*, H₂ pressure and temperature), incurs substantial costs, and is of limited efficiency for removing refractory sulfur compounds (*e.g.*, dibenzothiophene, DBT),⁵ which must be eliminated to comply with applicable regulations. In contrast, visible-light photo-driven ODS (or PODS) has gained significant attention due to its mild operating conditions, low energy requirements (using sunlight), enhanced safety (no hydrogen involved) and environmentally friendly character, demonstrating excellent efficiency in removing refractory sulfur compounds.⁶ Visible-light-driven ODS involves two main steps: (i) oxidation of sulfur-containing compounds into the corresponding sulfones by reactive oxygen species (ROS), generated from an oxidizing agent in presence of a photocatalyst under visible light irradiation, followed by (ii) extraction of the resulting sulfones.

Despite the promising potential of PODS, the development of efficient and robust photocatalysts remains crucial for advancing sustainable and cost-efficient desulfurization technologies. In this scenario, Metal-Organic Frameworks (MOFs) appear as promising candidates due to their chemical diversity and their easily tunable properties, although they might suffer from insufficient chemical stability and fast electron-hole recombination. While composite materials where the MOFs act as a host or a support of the active catalyst have been reported,^{7–10} the use of pure MOFs for PODS has been only recently investigated. For instance, the zeolitic imidazolate framework ZIF-67¹¹ and the Zr-based MOF NH₂-UiO-66,¹² which both possess a wide optical band gap (> 3 eV) were found to be active for the photocatalytic degradation of dibenzothiophene (DBT) under visible light irradiation in the presence of H₂O₂ as an oxidant. The Ti-based MOF MIL-125-NH₂, with a narrower band gap of 2.32 eV, demonstrated superior photocatalytic performance in ODS, achieving 70% DBT removal within 25 min.¹³ Inorganic vanadium-based materials (*e.g.*, V₂O₅-ZnO, Ag₃VO₄)^{14,15} have also demonstrated promising photocatalytic activity for PODS, in line with the ability of V to adopt several oxidation states and favor electron transfer. Although V-based MOFs are considered as potential candidates for photocatalytic processes in environmental applications,¹⁶ to the best of our knowledge, they have not yet been explored as photocatalysts for light-driven ODS, and their application in thermal-driven ODS has been scarcely reported.¹⁶ In the present work, we aimed at developing V-based MOFs presenting optimized optical absorption features and evaluating their PODS activity. We selected the ligand 2,5-disulfhydrylbenzene-1,4-dicarboxylic acid (H₄DSBDC), that not only absorbs light in the visible range through π - π^* transition but also can give rise to additional absorption through ligand-to-metal-charge transfer (LMCT) via M-S bonds. Although most MOFs based on DSBDC follow the Pearson's hard and soft acid and base (HSAB) theory,¹⁷ with materials based on M^I or M^{II} cations built through M-S and M-O bonds,^{18,19,20–22} meanwhile those based on M^{III} or M^{IV} are based exclusively on M-O bonds,^{20,23–28} we recently showed that Fe^{III} and DSBDC can give rise to stable materials comprising M-S bonds.^{29,30} With this in mind, we here evaluated the reactivity of the H₄DSBDC ligand with V^{III} and V^{IV} cations, leading to the successful synthesis of two new coordination polymers. The first solid, (DMA)KVO(DSBDC), presents coordination of V^{IV} to both O and S atoms, while the second is an analogue to the MIL-47(V), denoted MIL-47(V)-(SCH₃)₂, hence comprising only M-O bonds. The thermal features, chemical stability and optical properties of these materials are here reported, as well as their photocatalytic activities for the oxidation of DBT.

Results and discussion

Synthesis and physicochemical characterization



H₄DSBDC was prepared at the multi-gram scale following the reported protocol.³¹ Its reactivity with V salts was first systematically investigated using the high throughput solvothermal reactors developed by Stock et al.³² The nature of the solvent (water, alcohols, N,N-dimethylformamide-DMF and mixture) and vanadium precursors (V^{III}Cl₃, V^{IV}OSO₄, V^{IV}O(acac)₂), was investigated, as well as the effect of the time, temperature and addition of acids (HCl, acetic acid-AcOH) or bases (MOH, M = Li, Na, K). Two crystalline phases were identified, and their synthesis further up scaled for full characterization. It is worth to note here that the yield of both syntheses (75 and 95%, respectively) surpasses for more than twice, with some exceptions,^{33–35} the ones typically reported for V-based MOFs prepared under solvothermal conditions (< 40%).^{36–42}

The first solid was obtained from a mixture of VCl₃ and H₄DSBDC in DMF-water at 180 °C in presence of KOH (yield ≈ 75% based on V). Interestingly, the base has a strong influence of the reaction output: only amorphous solids were obtained when using LiOH or NaOH instead of KOH, in line with the crystal structure (see below). Amorphous solids were also obtained upon the addition of extra base (4 or 6 equivalents instead of 2) or when using a mixture of solvents (i.e. methanol and DMF) (Table S1). On the other hand, the vanadium precursor has only a minor influence on the result, since the same material can be obtained by using V^{III}Cl₃ or V^{IV}O(acac)₂, although in the latter case a smaller particle size and mixture of phases were observed (Figure S1). The micrometric size of the obtained crystals (~50 μm, Figure S2) allowed the elucidation of the crystalline structure by using conventional single crystal X-ray diffraction (SC-XRD). The material, formulated (C₂H₈N)KVO(C₈H₂O₄S₂) and denoted (DMA)KV^{IV}O(DSBDC), crystallizes in the triclinic space group *P*-1 with *a* = 6.9416(5) Å, *b* = 10.3763(7) Å, *c* = 10.4436(7) Å, α = 101.025(6)°, β = 101.363(6)°, γ = 98.543(6)° and *V* = 710.19(9) Å³ (Tables 1 and S2; CCDC n° 2246050). The structure consists of fully deprotonated ligand DSBDC⁴⁻ (Figure 1a) bound to vanadium and potassium to define an anionic network with entrapped dimethylammonium (DMA) cations. Note that the presence of such an organic cation can be easily rationalized considering the DMF decomposition, as already reported for other MOFs prepared in similar synthetic conditions.⁴³ The vanadium ions are connected to two DSBDC linkers by both O and S atoms through 6-membered chelate rings (Figure 1b) that define the square-base of a pyramid with the V ion at the center. The apical position is occupied by an O atom, giving rise to the coordination motif VO₃S₂. The V-O apical distance is significantly shorter than the equatorial ones (1.59 and ~ 1.95 Å, respectively), indicating the formation of a vanadyl V=O bond, which is characteristic of V^{IV} complexes.^{44,45} The oxidation state of the vanadium is further confirmed by bond valence calculations (BVC, Table 2)⁴⁶ and charge balance consideration. The resulting anionic {VO(DSBDC)²⁻}_n chains further interact with K⁺ cations (*d*_{K-O} = 2.61 – 3.2 Å; *d*_{K-S} ~ 3.31 Å, Figure S4), resulting in a 3D network with 1D channels (~8 × 4 Å² considering Van der Waals radii of the atoms). The alkali ions are thus part of the hybrid framework; considering the ionic radii of Li, Na and K (0.9, 1.16 and 1.52 Å, respectively), this probably explains why the framework could not be obtained with the smaller alkali. DMA cations are disordered within the cavities, establishing N-H...O hydrogen bonds with the carboxylate and vanadyl moieties. Finally, the purity of the polycrystalline samples prepared from VCl₃ was assessed by Rietveld refinement (Figure S7 and Table S4) and elemental analysis (see SI for further details), both indicating the absence of any impurity.

Table 1. Unit cell parameters of (DMA)KVO(DSBDC) and MIL-47(V)-(SCH₃)₂.

Compound	(DMA)KVO(DSBDC)	MIL-47(V)-(SCH ₃) ₂
Chemical formula	(C ₂ H ₇ N)KVO(C ₈ H ₂ S ₂ O ₄)	VOH(C ₁₀ H ₈ S ₂ O ₄)
Crystal system	Triclinic	Monoclinic
Wavelength	0.71073 Å	0.671415 Å
Space group	<i>P</i> -1	<i>C</i> 2/ <i>c</i>
<i>a</i>	6.9416(5) Å	18.9190(4) Å



<i>b</i>	10.3763(7) Å	11.6119(3) Å	View Article Online DOI: 10.1039/D5QI02257F
<i>c</i>	10.4436(7) Å	6.87187(2) Å	
α	101.025(6) °	-	
β	101.363(6) °	108.9768(1) °	
γ	98.543(6) °	-	
<i>V</i>	710.19(9) Å ³	1427.60(7) Å ³	
<i>M</i> ₂₀	-	87	
<i>Z</i>	2	4	

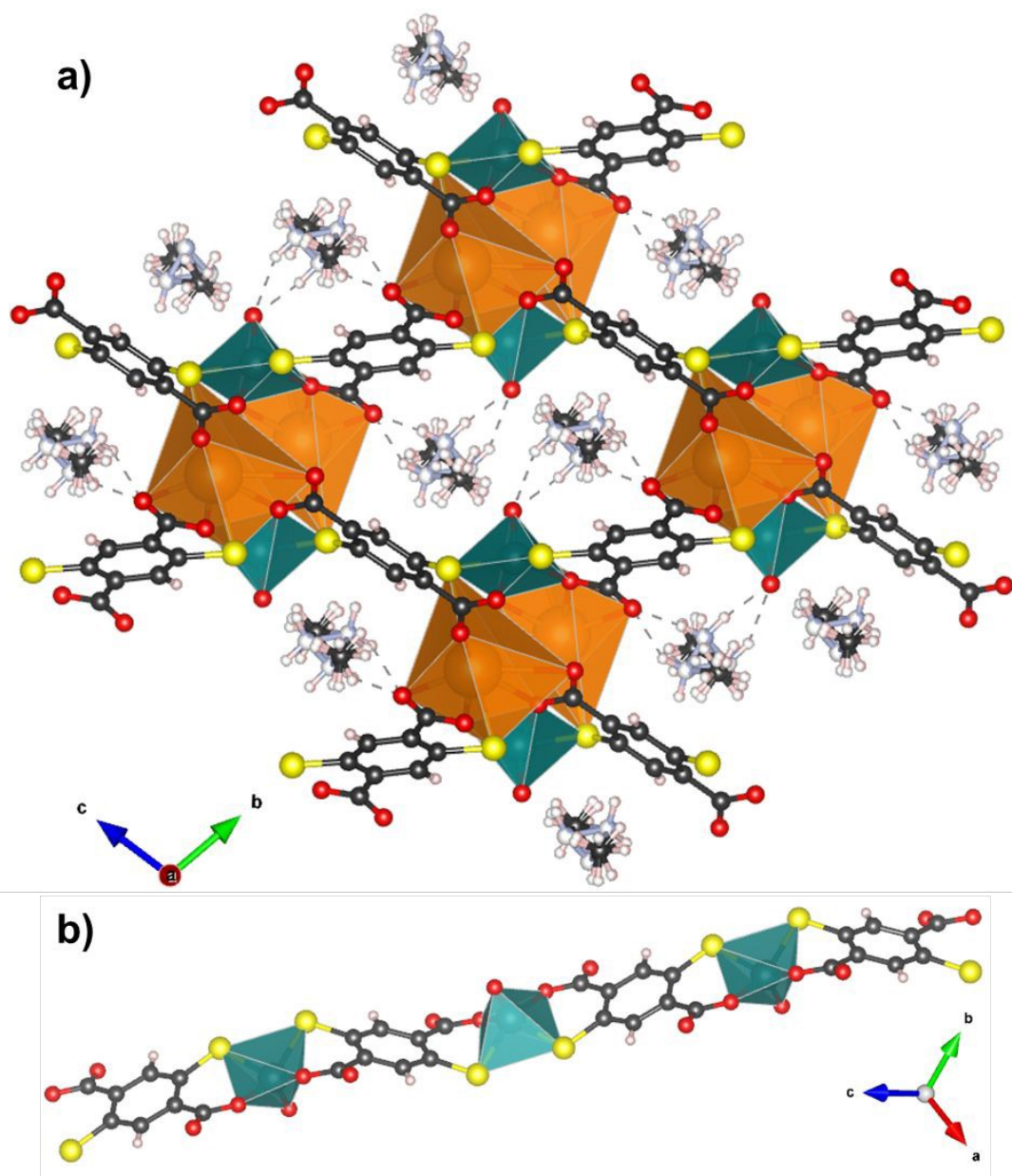


Figure 1. Crystalline structure of (DMA)KVO(DSBDC): a) view along *a* axis and b) representation of the VO(DSBDC) 1-D chain. Vanadium, potassium, sulfur, oxygen, nitrogen, carbon and hydrogen represented in dark green, orange, yellow, red, pale blue, black and white, respectively.





The second phase was obtained by reacting the H₄DSBDC and V^{III}Cl₃ in a mixture of DMF and methanol (MeOH) at 180 °C for 50 h (yield = 95% based on V). Unlike the (DMA)KVO(DSBDC) material, this second phase cannot be obtained by using V^{IV}O(acac)₂ as precursor. The DMF:MeOH solvent proportion was systematically varied from 9:1 to 5:5), and a ratio of 8:2 was found to be optimal (Table S1 and Figure S6). The replacement of methanol by other alcohols (ethanol, isopropanol) led to unidentified or amorphous phases (Table S1). The solid was initially obtained in the form of small crystallites (~0.5 μm, Figure S3); attempts were carried out to increase the size of the crystals, including the use of mineralizing agents (HF) and modulators (AcOH), and increasing the metal concentration (from 0.05 to 0.2 M). This allowed growing larger needle-like crystals of up to 10 μm (Figure S3), but still too small for SC-XRD. The crystal structure was then elucidated by synchrotron powder X-ray diffraction (PXRD). The material crystallized in the monoclinic space group *C2/c* with *a* = 18.9190(4) Å, *b* = 11.6119(3) Å, *c* = 6.87187(2) Å, *β* = 108.9768(1)°, and *V* = 1427.60(7) Å³ (Figure S8 and Table S3; CCDC n° 2497420). This phase exhibits a porous structure similar to that of the well-established MOF MIL-47(V) (Figure 2a),^{36,47} where chains of VO₆ octahedra sharing vertexes (Figures 2b and S5) are connected by the terephthalate ligands, creating channels along the *c* axis with an approximate size of 8 x 5.5 Å (considering the Van der Waals radii of the atoms) that contain disordered DMF molecules representing 27% of the unit cell volume according to PLATON calculations. BVC (Table 2) confirmed the oxidation state of V as +III in the as-synthesized compound, similarly to what is found in the non-functionalized MIL-47(V) material. The ligand is thus bound to the V^{III} ions through the O atoms only, but interestingly, the obtained material is not MIL-47(V)-(SH)₂, as could be expected by using the thiol-functionalized version of the terephthalate linker, but rather corresponds to the thiomethyl-functionalized version of the material (labeled as MIL-47(V)-(SCH₃)₂), with formula V^{III}OH(Me₂DSBDC)·(guest) confirmed by elemental analysis (see SI). The linker methylation occurred by an irreversible *in situ* condensation reaction with methanol.

Table 2. V-O and V-S bond distances and bond valence calculations for the obtained materials.

Compound	Bond	Distance (Å)	Bond valence	V ox. state	
(DMA)KVO(DSBDC)	V-O	1.955(4)	0.65	4.11	+4
	V-O	1.965(3)	0.60		
	V-O _{vandyl}	1.598(4)	1.44		
	V-S	2.3357(1)	0.74		
	V-S	2.3650(1)	0.68		
MIL-47(V)-(SCH ₃) ₂	V-O (x2)	1.936(4)	0.59	3.18	+3
	V-O (x2)	2.009(9)	0.48		
	V-O (x2)	1.991(8)	0.51		

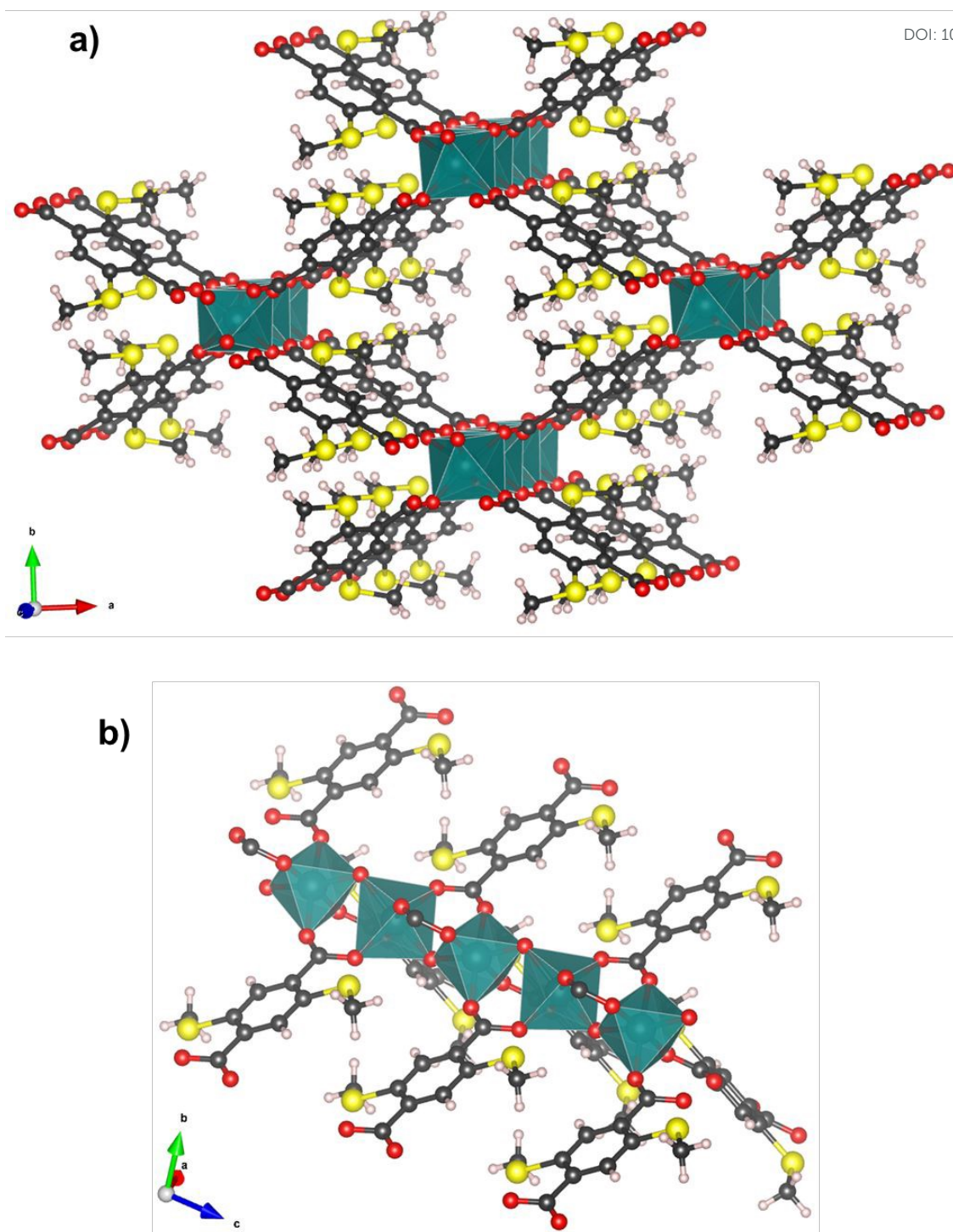


Figure 2. Structure of MIL-47(V)-(SCH₃)₂ (a) and representation of the VO₆ chains (b). Vanadium, sulfur, oxygen, carbon and hydrogen represented in dark green, yellow, red, black and white, respectively. Entrapped DMF molecules were omitted for the sake of clarity.

MIL-47(V)-(SCH₃)₂ is then exclusively built up from V-O coordination bonds. In contrast, in the (DMA)KVO(DSBDC) material, both the carboxylate and thiolate groups are bound to the V^{IV} cation. Although this reactivity is not what is expected based on the HSAB theory,¹⁷ it agrees with the experimental observation in discrete coordination compounds, where the coordination of both hard (carboxylate) and soft (thiolate) groups of the linker to M^{III/IV} cations was sometimes observed upon the addition of a base to the reaction medium.^{48–51} This reactivity has also been recently reported by our group for a series of layered materials formulated AFe(DSBDC) (A = Na, K, DMA), in which both S



and O atoms from the DSBDC linker coordinate to the Fe^{III} center.²⁹ Interestingly, although the synthetic conditions are comparable and the coordination mode identical (metallic cation chelated through a 6-membered ring involving both the carboxylate and thiolate functions), the structures of the V- and Fe-based solids are markedly different. This can be easily explained considering the *in situ* oxidation of the V^{III} to create the VO^{2+} specie, leading to isolated square-based VS_2O_3 pyramids instead of the FeS_4O_2 edge-sharing octahedra found in $\text{AFe}(\text{DSBDC})$.

These different coordination modes are in agreement with the Fourier transformed infrared (FTIR) spectroscopy analysis. As can be seen in Figure S12, when compared to the pristine ligand H_4DSBDC , one of the most significant differences is observed for the carboxylic/ate ν elongation bands in the 1700–1500 cm^{-1} region. For H_4DSBDC , a single band is observed at 1680 cm^{-1} , corresponding to the $\text{C}=\text{O}$ bond. For $(\text{DMA})\text{KVO}(\text{DSBDC})$, two bands are observed at lower wavenumbers (1616 and 1582 cm^{-1}), in line with the interaction of the carboxylate group with the $\text{V}(\text{IV})$ and K ions. For $\text{MIL-47}(\text{V})-(\text{SCH}_3)_2$, a single band is found at lower wavenumber (1541 cm^{-1}), as a consequence of the bonding to the V^{III} ions. This analysis supports the fact that the environment of the carboxylate moieties are very different in both MOFs. Another relevant difference is found for the ν C-S bands. In the spectra of both H_4DSBDC and $(\text{DMA})\text{KVO}(\text{DSBDC})$, a single band appears at 634 and 627 cm^{-1} , respectively, and is attributed to the $\text{S}-\text{C}_{\text{arom}}$ bond. In contrast, the spectrum of $\text{MIL-47}(\text{V})-(\text{SCH}_3)_2$ exhibits two bands at 654 and 598 cm^{-1} , attributed to the $\text{S}-\text{C}_{\text{arom}}$ and $\text{S}-\text{CH}_3$ bonds, confirming the alkylation of the S atoms during the synthesis. Additional attribution of the IR vibration bands can be found in Table S5.

The thermal stability of the materials was assessed by thermogravimetric analysis (TGA) and variable temperature PXRD (VT-PXRD) under air, while the porosity was evaluated by N_2 sorption experiments at 77 K. For $(\text{DMA})\text{KVO}(\text{DSBDC})$, no weight loss was detected of the TGA curve before 290 °C, in line with the absence of volatile species in the structure. Above this temperature, a continuous weight loss is observed up to 610 °C, and associated to the decomposition of the solid (Figure S15). In good agreement with this, VT-PXRD experiments showed that the crystalline structure was maintained with no noticeable structural modification up to 280 °C, becoming amorphous at higher temperature when the decomposition started (Figure S16). Both experiments confirmed the structural role of the DMA cations, which cannot be removed without compromising the structural integrity of the material. This was further confirmed by N_2 sorption experiments that evidenced no accessible porosity for this compound.

Two forms of $\text{MIL-47}(\text{V})-(\text{SCH}_3)_2$ were studied: the pristine solid, that contain DMF molecules in the pores (see above), and the MeOH-exchanged material. This latter was obtained by suspending the pristine material in MeOH (see experimental section for further information). IR spectroscopy confirmed the complete removal of the DMF molecules (Figure S13), while the PXRD patterns and unit-cell parameters of both compounds presents slight differences (Figure S9), in line with the structural flexibility of the MIL-47 materials (see below). The TGA curve of pristine $\text{MIL-47}(\text{V})-(\text{SCH}_3)_2$ (Figure S17) displayed an initial weight loss of around 10% from room temperature (RT) to 200 °C, which corresponds to the DMF departure, followed by a second weight loss from 250 to 550 °C, attributed to the material decomposition. The material suspended in MeOH presents a slightly different TG curve (Figure S19), with the decomposition occurring at 250 °C and solvent departure completed at 80 °C, in line with the lower boiling point of MeOH compared to DMF. In both cases, VT-PXRD data supported these findings, revealing an amorphization temperature for both solids of ~250 °C, associated to the degradation of the framework (Figures S18 and S20). Below this temperature, a continuous shift of the diffraction peaks is observed whatever the initial pore content. Additional VT-PXRD experiments performed on the MeOH exchanged sample showed that this behavior is reversible when the experiment is carried out under N_2 (Figure S22), but not when done under air (Figure S21). These results can be rationalized in view of the behavior of MIL-47.^{36,47} MIL-47 is formulated in its pristine state $\text{V}^{\text{III}}(\text{OH})(\text{BDC})\cdot(\text{guest})$. Similarly to the isostructural MIL-53(M) (or $\text{M}(\text{OH})(\text{BDC})$, M = Al, Cr, Fe, Ga) solid, this MOF presents a high structural flexibility, associated with the existence of two extreme pore opening, the close pore (CP) and large pore (LP) forms. When exposed to air at 200 °C, V^{III} is



oxidized to V^{IV} , and the resulting solid formulated $V^{IV}O(BDC)$ becomes rigid. In the present case, the shift of the diffraction peaks observed when heating MIL-47(V)-(SCH₃)₂ can be associated to structural flexibility, as expected for a reduced V^{III} form. Note nevertheless that the shift is moderate, indicating a flexibility of lower amplitude than that of $V^{III}(OH)(BDC) \cdot (guest)$. This phenomenon is expected for MIL-53 type framework functionalized by bulky groups that prevent the complete breathing of the pore because of their steric hindrance.^{52,53} The fact that this flexibility is not reversible when the experiment is carried out under air suggests at first sight an oxidation into $V^{IV}O(Me_2DSBDC)$ that becomes rigid, similarly to $V^{IV}O(BDC)$. Nevertheless, a partial degradation could also explain the irreversible diffraction peak broadening: the FTIR spectrum of the product after the thermal treatment (Figure S14) indeed presents significant modification, including new bands at ~1170, 1230, ~1700 and ~3300 cm⁻¹ associated to -SO₃H symmetric and asymmetric stretching, C=O and O-H vibrations, respectively, and the disappearance of the bands at ~2900 cm⁻¹ and ~650 cm⁻¹ associated to the -SCH₃ group that suggests an irreversible oxidation of the organic ligand. The porosity of the MIL-47(V)-(SCH₃)₂ was confirmed experimentally by N₂ sorption on the MeOH-exchanged material. As expected, the solid presents a type I isotherm (Figure S10), with $S_{BET} = 450 \text{ m}^2 \cdot \text{g}^{-1}$ and $V_p = 0.18 \text{ cm}^3 \cdot \text{g}^{-1}$. Horvath-Kawazoe pore size distribution (Figure S11) showed a pore diameter around 6 Å, which fairly agrees with the crystallographic pore size (8 x 5.5 Å, see above). The minor difference could be rationalized considering the flexibility of the structure observed during the activation of the solid, which might also be evidenced by the change of slope observed in the low-pressure range of the N₂ sorption isotherm (Figure S10). In comparison with the non-functionalized version (MIL-47(V)),³⁶ the MIL-47(V)-(SCH₃)₂ presents roughly the half of the surface area and pores volume, in line with the presence of the bulky methylthio (-SCH₃) groups into the pores.

Eventually, the chemical stability of the materials was also evaluated by suspending a controlled amount of powdered samples (2 mg mL⁻¹) in water and in a variety of industrially relevant organic solvents (*i.e.* ethanol-EtOH, MeOH, tetrahydrofuran-THF, acetonitrile-ACN, DMF and hexane) under stirring overnight. The structural integrity was then evaluated by PXRD (Figure S23 and S24 for (DMA)KVO(DSBDC) and MIL-47(V)-(SCH₃)₂, respectively). While (DMA)KVO(DSBDC) is stable only in organic solvents and dissolved in water, the MIL-47(V)-(SCH₃)₂ retained its structure under all tested conditions. Here again, the flexibility of MIL-47(V)-(SCH₃)₂ was evidenced by the changes observed in the PXRD pattern upon immersion in DMF, which reverted to the pristine PXRD pattern after solvent exchange.

Optical characterization

The optoelectronic properties of both materials, as well as the free ligand H₄DSBDC, were evaluated using diffuse reflectance (DR) UV-Vis spectroscopy in the 200-800 nm range (Figure 3 and Figure S25). H₄DSBDC ligand presents at low reflectance (hence high absorbance), from 200 to ~450 nm, likely associated to $\pi-\pi^*$ transitions. Both MOFs also absorb light in the visible range, but with different features. For MIL-47(V)-(SCH₃)₂, light is absorbed from 200 up to 550 nm; this can be associated to the ligand-centered $\pi-\pi^*$ transition (see above) together with additional V^{III} centered d-d transitions. These features are also found for (DMA)KVO(DSBDC), but an additional broad band spanning from ~550 to at least 800 nm is also visible. This last band is likely associated to LMCT, similarly to what is found in analogous vanadium-phenolate complexes,^{45,50} but here through V-S bonds. The optical band gaps were estimated using Tauc plots, reaching 2.19 and 2.43 eV for MIL-47(V)-(SCH₃)₂ and (DMA)KVO(DSBDC), respectively (Figure S27 and S26). These values should nevertheless be considered with caution, knowing that the reflectance spectra involve multiple contribution as discussed above. In addition, photoluminescence (PL) experiments were conducted using an excitation of 415 nm (Figure S28), revealing that both materials exhibit an emission band at 510 nm, possibly with a slightly lower intensity for MIL-47(V)-(SCH₃)₂.



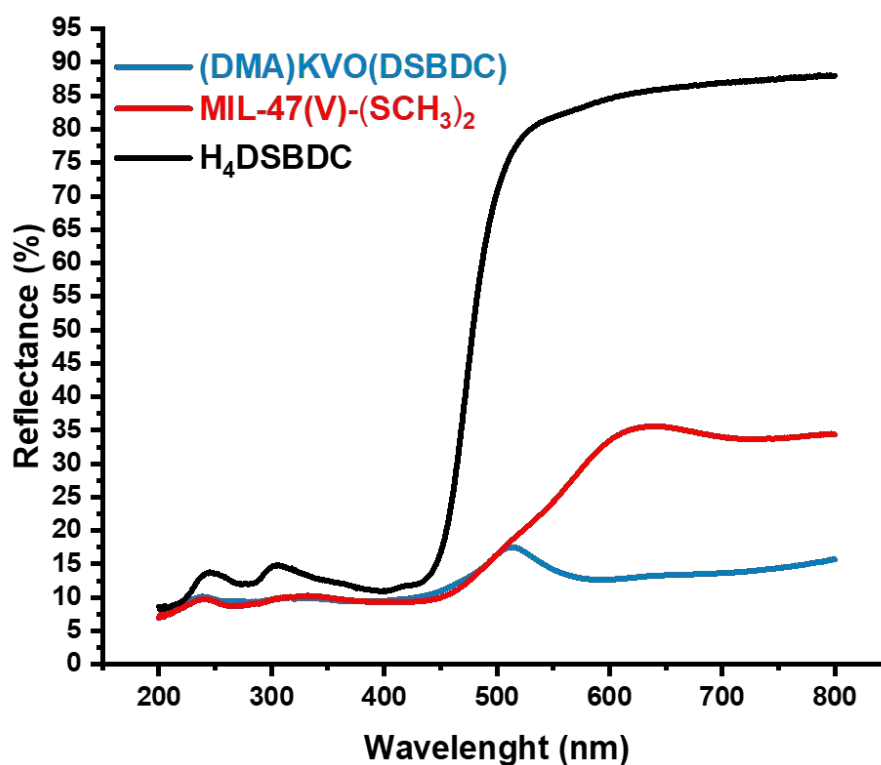


Figure 3. DR-UV-Vis spectra of (DMA)KVO(DSBDC) (blue), MIL-47(V)-(SCH₃)₂ (red) and H₄DSBDC ligand (black).

Photocatalytic desulfurization

Considering their chemical stability and strong light absorption in the visible range, (DMA)KVO(DSBDC) and MIL-47(V)-(SCH₃)₂ were evaluated as photocatalysts for the PODS of DBT, using H₂O₂ as an oxidant and visible light as the energy source (Table 3). The evolution of the amount of both DBT and its oxidation product DBT sulfone (Scheme S1) was followed by high performance liquid chromatography (HPLC). As the reaction could not be carried out directly in oil due to the poor dispersion of the MOF in this apolar medium and extraction issues, initial tests were conducted in a liquid-solid phase system based on ACN, in which the MOFs are stable (see above) and easily dispersed. This allowed comparing the visible-light-driven photocatalytic activity of both materials while minimizing mass transfer limitations encountered in liquid-liquid-solid phase system (L(ACN)-L(oil)-S(catalyst), see below). A reaction time of 3 h was selected, in line with previous studies on V-based MOFs for thermally-driven ODS.⁵⁴ Control experiments performed in the absence of the MOF photocatalyst and with various amounts of H₂O₂ (H₂O₂ / DBT molar ratio = 3 and 6, Entries 1 and 2, respectively) resulted in negligible DBT removal. Furthermore, adsorption and oxidation tests using MIL-47(V)-(SCH₃)₂ in the dark (Entries 3 and 4) revealed the limited DBT adsorption capacity of the material, and only a minor amount of the oxidation product (7.2 ± 0.9 %). In the absence of photocatalyst and under dark conditions, only DBT extraction into the polar phase was observed (blank P, Figure 4a), with a DBT removal of 44 ± 3 %, and no DBT sulfone detected in the ACN phase. A blank thermal experiment at room temperature without photocatalyst resulted in only DBT extraction, with no sulfone formation (blank TC, Figure 4b).

In contrast, under visible light, both MIL-47(V)-(SCH₃)₂ and (DMA)KVO(DSBDC) displayed significant DBT removal (*i.e.* 23.8 ± 1.1 % and 20.2 ± 1.0 %, respectively) using an H₂O₂/DBT molar ratio of 3 (Entries 5 and 7). When doubling the amount of oxidant (H₂O₂/DBT = 6), the removal of DBT increased further, reaching 41.8 ± 1.4 % and 44.5 ± 2.6 % for MIL-47(V)-(SCH₃)₂ and



(DMA)KVO(DSBDC), respectively (Entries 6 and 8), indicating a positive correlation between the concentration of oxidant and the photocatalytic performance. Note that both materials exhibited comparable photocatalytic activity at 3 h, suggesting that the additional LMCT visible light absorption path for (DMA)KVO(DSBDC) does not play a significant role in the photocatalytic process.

Furthermore, the structural integrity of both photocatalysts after the reaction was evaluated by PXRD (Figure S29 and S30). Both MOFs retained their crystallinity under low oxidant concentration (H_2O_2 / DBT = 3). However, under high oxidant concentration (H_2O_2 / DBT = 6), a broadening of the diffraction peak is observed for (DMA)KVO(DSBDC), suggesting a partial degradation.

Table 3. DBT removal and yield of DBT sulfone using V-MOF photocatalysts.

Entry	Photocatalyst	H_2O_2 / DBT molar ratio	Irradiation	Removal of DBT (%) ^d	Yield of DBT sulfone (%) ^d
1	-	3	Yes	-	-
2	-	6	Yes	-	-
3	MIL-47(V)-(SCH ₃) ₂ ^a	-	No	-	-
4	MIL-47(V)-(SCH ₃) ₂ ^b	3	No	16 ± 1	7.2 ± 0.9
5	MIL-47(V)-(SCH ₃) ₂ ^c	3	Yes	24 ± 1	15 ± 2
6	MIL-47(V)-(SCH ₃) ₂ ^c	6	Yes	42 ± 1	40 ± 1
7	(DMA)KVO(DSBDC) ^c	3	Yes	20 ± 1	13 ± 1
8	(DMA)KVO(DSBDC) ^c	6	Yes	44 ± 3	38 ± 2

^a Reaction conditions: 20 mg of photocatalyst, 10 mL of a solution of 575 ppm DBT in ACN, under darkness and in the absence of H_2O_2 for 3 h. ^b Reaction conditions: 20 mg of photocatalyst, 10 mL of a solution of 575 ppm DBT in ACN, under darkness for 3 h. ^c Reaction conditions: 20 mg of photocatalyst, 10 mL of a solution of 575 ppm DBT in ACN, under visible irradiation for 3 h. ^d DBT removal and yield of DBT sulfone determined by HPLC.

Kinetic studies for both V-based photocatalysts were performed under optimized conditions (*i.e.*, H_2O_2 / DBT molar ratio = 6). As can be seen in Figure S31, DBT removals of 43 ± 2 and 41 ± 2 % were achieved within 30 min for MIL-47(V)-(SCH₃)₂ and (DMA)KVO(DSBDC), respectively, corresponding to DBT sulfone yields of 39 ± 1 % and 37 ± 2 %. Notably, MIL-47(V)-(SCH₃)₂ reached a DBT sulfone yield of 40 ± 2 after just 15 min, significantly higher than that of (DMA)KVO(DSBDC) (27 ± 1.1 % in 15 min), indicating a faster DBT oxidation rate for MIL-47(V)-(SCH₃)₂ compared to (DMA)KVO(DSBDC). This enhanced oxidative performance is likely not related to the microporosity of MIL-47(V)-(SCH₃)₂ (pore size is not in favor of fast DBT diffusion), but rather results from its higher external surface exposed to DBT, arising from the lower particle size and possibly a lower recombination rate of photogenerated electron-hole pair, as suggested by the photoluminescence (PL) analysis.

To evaluate the photocatalytic performance of the V-based MOFs in conditions closer to practical applications, experiments were conducted in a liquid-liquid-solid phase system (L(ACN)-L(oil)-S(catalyst)), using a mixture of 10 mL of a model oil (a solution of DBT in *n*-octane) and 5 mL of ACN,



in the presence of H_2O_2 as an oxidant (H_2O_2 / DBT molar ratio = 6), under visible light irradiation for 3 h (Figure 4a). In the absence of photocatalyst, only extraction of DBT into the polar phase was observed (blank P, Figure 4a) with a DBT removal of 44 ± 3 %, and no DBT sulfone detected in this phase. Upon addition of the photocatalyst, DBT removal efficiencies of 66 ± 3 % and 63 ± 2 % were achieved for MIL-47(V)-(SCH₃)₂ and (DMA)KVO(DSBDC), respectively. Analysis of the acetonitrile phase confirmed the oxidation of DBT into DBT sulfone, with yields of ca. 40% for both materials, suggesting comparable photocatalytic activities under tested conditions.

Additionally, thermal-driven ODS experiments were also performed to investigate the influence of the energy source (Figure 4b). Based on previously reported studies on V-MOFs used for thermal-driven ODS,^{55,56} the temperature was set at 60 °C. A blank thermal experiment was carried out at room temperature in the absence of catalyst, resulting in only DBT extraction, with no sulfone formation (blank TC, Figure 4b). In contrast, in the presence of the catalyst, similar DBT removal efficiencies were obtained for both MOFs (54.2 ± 0.3 % and 52.1 ± 0.7 % for MIL-47(V)-(SCH₃)₂ and (DMA)KVO(DSBDC), respectively). However, the corresponding DBT sulfone yields were lower (30.9 ± 0.3 % and 27.8 ± 1.9 %) than those obtained under visible light irradiation, indicating that visible-light activation enhances the oxidative performance of both catalysts compared to purely thermal conditions.

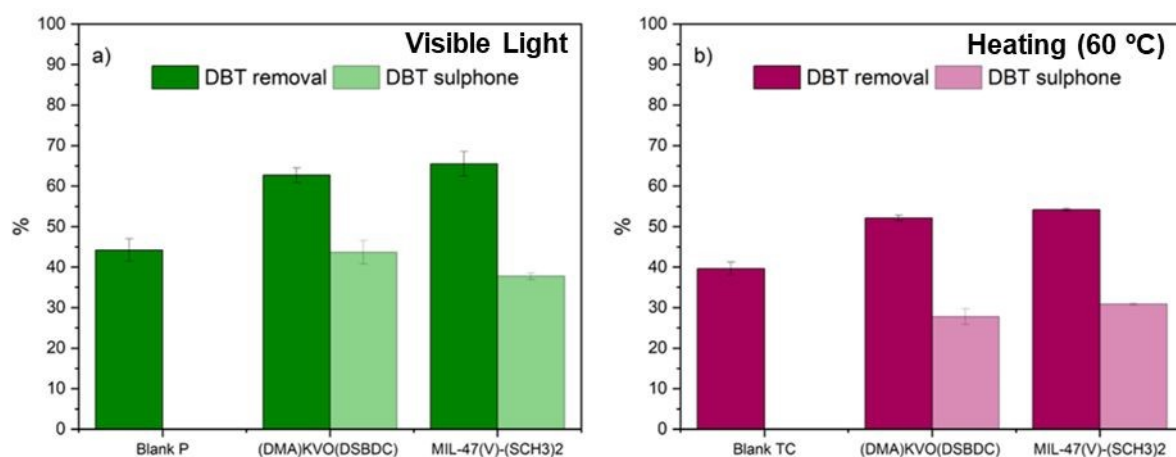


Figure 4. Comparison of a) photocatalytic (P) and b) thermal catalytic (TC) performance of (DMA)KVO(DSBDC) and MIL-47(V)-(SCH₃)₂ for DBT removal efficiency and DBT sulfone yield. Reaction conditions: 20 mg of catalyst, 10 mL of a solution of 575 ppm DBT in n-octane, 5 mL of ACN, 20 μL of a solution 30% H_2O_2 and 3 h of visible irradiation (photocatalysis) or 60 °C for 3 h (thermal catalysis). Blank experiments, reaction conditions: 10 mL of a solution of 575 ppm DBT in n-octane, 5 mL of ACN, 20 μL of a solution 30% H_2O_2 under dark conditions (Blank P) and at room temperature (Blank TC).

The chemical stability of both V-based catalysts was evaluated by PXRD and ICP-MS after 3 and 6 h of reaction. While the PXRD pattern of MIL-47(V)-(SCH₃)₂ does not significantly evolve (Figure S33), that of (DMA)KVO(DSBDC) is significantly modified, with new diffraction peaks appearing after 6h of reaction (Figure S32). ICP-MS analysis further revealed a significant leaching of vanadium for this material (7.3 ± 0.4 % and 47.3 ± 0.6 % after 3 and 6 h of reaction, respectively), while the loss is negligible for MIL-47(V)-(SCH₃)₂ (2.7 ± 0.5 % and 2.6 ± 0.9 % after 3 and 6 h of reaction, respectively), confirming its superior chemical stability. Based on these results, MIL-47(V)-(SCH₃)₂ was selected as the best photocatalyst for further analyses. The effect of light exposure time and oxidant concentration was subsequently investigated. DBT removal efficiency of MIL-47(V)-(SCH₃)₂ increased with reaction time, from 57 ± 2 % at 30 min to 66 ± 3 % at 3 h (see Figure S34). When the reaction time was fixed to 60 min and the oxidant concentration was doubled (H_2O_2 / DBT molar ratio = 12), DBT removal



improved significantly ($61 \pm 2\%$ vs. $72.7 \pm 0.1\%$, respectively). Thus, the highest DBT removal efficiency ($72.7 \pm 0.1\%$) was achieved at a H_2O_2 /DBT molar ratio of 12 and a reaction time of 60 min. Article Online
DOI: 10.1039/D5QI02257F

Comparison with other reported MOF-based photocatalysts shows that MIL-47(V)-(SCH₃)₂ competes with best behaving materials (Table 4) without the addition of any co-catalyst.

Table 4. Performance comparison between different MOFs and MOF-based composites in PODS.

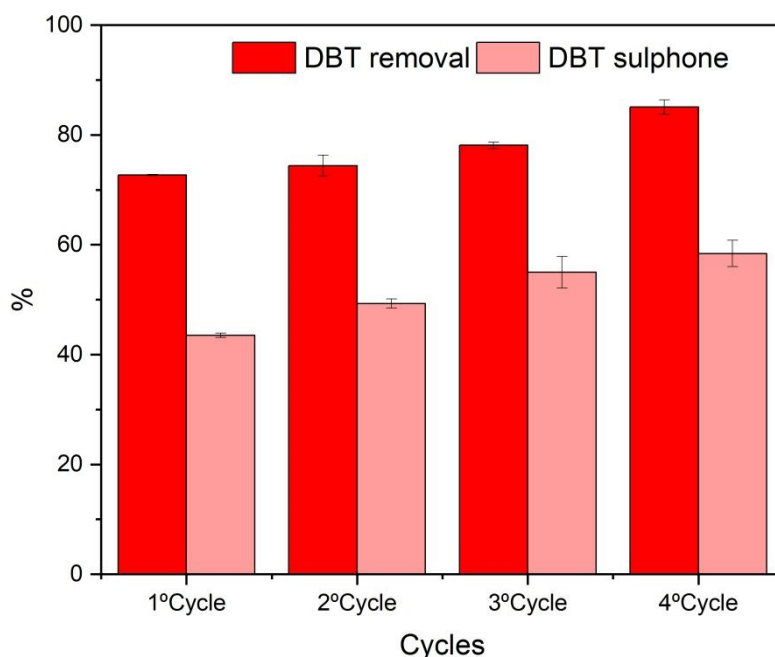
Material	Mass of catalyst (mg)/Volume or reaction (mL)	Oxidant / DBT molar ratio	DBT concentration (ppm)	Time (min)	Temperature (°C)	Removal (%)	Ref
MIL-47(V)-(SCH ₃) ₂	20/10	12 ^a	575	60	RT	73	This work
HKUST-1	10/n.a.	10 ^a	100	20	RT	39	8
BiVO ₄ @HKUST-1	10/n.a.	10 ^a	100	20	RT	55	8
ZIF-67	80/80	8 ^a	500	60	30	65	11
MIL-125-NH ₂	10/7	5 ^{a,b}	1000	25	30	35	13
MIL-101(Fe)	90/180	3 ^a	500	30	RT	45	57
0.133CeO ₂ /MIL-101(Fe)	90/180	3 ^a	500	30	RT	45	57
UiO-66-NH ₂	20/50	- ^b	250	90	RT	25	12
Ce-UiO-66-NH ₂	20/50	- ^b	250	90	RT	35	12

^a H₂O₂; ^b O₂. n.a.: not available.

Furthermore, when compared with other V-based MOF catalysts used in thermal-driven ODS, MIL-47(V)-(SCH₃)₂ demonstrated improved DBT removal efficiency. The mesoporous vanadium(III) trimesate MIL-100(V) indeed showed 72% DBT removal at 60 °C for 2 h using H₂O₂ (O/S ratio = 8) as the oxidant.⁵⁵ The pristine MIL-47(V) achieved 34.8 % DBT removal at 120 °C for 3 h⁵⁴ and 55 % at 60 °C for 2 h⁵⁸ using oxygen and tert-butyl hydroperoxide (TBHP) as oxidants, respectively, suggesting that the SCH₃ functionalization has a positive impact of the activity of MIL-47(V). Overall, these comparisons highlight the efficiency of MIL-47(V)-(SCH₃)₂ under visible-light-driven conditions, offering a more sustainable and energy-efficient alternative compared to conventional thermal-driven ODS processes.

Finally, the reusability of MIL-47(V)-(SCH₃)₂ was evaluated under the optimized reaction conditions. 4 successive cycles were carried out. A good cyclability of the photocatalyst was observed, with DBT removal efficiencies exceeding 70% during the first 3 cycles, followed by a further increase during the 4th cycle ($85 \pm 1\%$). The stability of the MOF was then evaluated by PXRD (Figure S35), FTIR (Figure S36), ICP-MS (Table S6) and morphological analysis (Figure S37). As can be seen in the Figure S35, although the diffraction peaks corresponding to the MOF structure were retained, a broadening is observed after the 4th cycle, suggesting a partial degradation of MIL-47(V)-(SCH₃)₂ upon extended use. This was further confirmed by FTIR (Figure S36), which revealed the appearance of the new bands at 1700 and 1143 cm⁻¹, associated to free carboxylic groups and possibly S=O bonds, respectively, and thus suggesting a partial degradation of the framework and oxidation of the ligand. Finally, ICP-MS (Table S6) revealed only a slight, but continuous, release of vanadium (from 3.9 % to 10.7 % in the 1st and 4th cycle, respectively). The enhanced activity during the last cycle might hence be related with an increase of vanadium exposed sites as a consequence of the ligand leaching and oxidation and consequently partial amorphization of the MOF particles.





View Article Online
DOI: 10.1039/D5QI02257F

Figure 5. DBT removal efficiency and DBT sulfone yield across consecutive 60-min photocatalytic cycles using MIL-47(V)-(SCH₃)₂

Conclusions

Two novel V-based MOFs were successfully synthesized and comprehensively characterized. Both materials are constructed from the DSBDC ligand, which displayed distinct coordination modes depending on the synthetic conditions. The addition of a base afforded (DMA)KVO(DSBDC), in which ligand binds to V(IV) through both S and O atoms, while the use of DMF/MeOH mixture promoted the formation of the porous MIL-47(V)-(SCH₃)₂, a functionalized analogue of the MIL-47(V) containing -SCH₃ functional groups derived from an *in situ* condensation reaction. Both materials presented good chemical stability in various organic solvents, that, combined with their ability to absorb light in the visible range, makes them suitable candidates as photocatalysts for the PODS reaction, reaching ~60% of DBT removal in the L-L-S system. Among them, MIL-47(V)-(SCH₃)₂ showed superior performance and chemical stability compared to (DMA)KVO(DSBDC). Upon optimization of the reaction conditions, MIL-47(V)-(SCH₃)₂ achieved 72% of DBT removal, maintaining its activity during 4 cycles. These results pave the way for the development of new V-based photocatalysts for PODS, providing that their long-term stability can be improved.

Experimental methods

Synthetic procedures:

All the chemicals were purchased from Merck-Sigma Aldrich and used as received without further purification. VCl₃ (97%, 157.3 g·mol⁻¹), VO(acac) (98%, 265.16 g·mol⁻¹), KOH (85%, 56.11 g·mol⁻¹), DMF (ACS reagent, ≥ 99.8%), MeOH (ACS reagent, ≥ 99.8%). H₄DSBDC was synthesized using the reported procedure.³¹

Synthesis of (DMA)KVO(DSBDC) or (C₂H₈N)KVO(C₈H₂O₄S₂) (MW = 378.35 g·mol⁻¹): In a 23 mL Teflon-lined reactor, 115.08 mg of H₄DSBDC (0.5 mmol) and 78.6 mg of VCl₃ (0.5 mmol) were dissolved into 9 mL of DMF. Then, 1 mL of a KOH 1M aqueous solution were added dropwise. The



mixture was heated at 180 °C during 16 h. The obtained dark green crystals were recovered by filtration and washed with DMF, H₂O and EtOH and dried under air (~140 mg recovered).

For the solid prepared using VO(acac)₂, the same procedure was followed, adding 132.5 mg of VO(acac)₂ (0.5 mmol) instead of VCl₃.

Synthesis of MIL-47(V)-(SCH₃)₂ or V^{III}OH(C₁₀H₈O₄S₂) (MW dry = 324.24 g·mol⁻¹): In a 16 mL Teflon-lined reactor, 476.4 mg of H₄DSBDC (2.07 mmol) and 217.1 mg of VCl₃ (1.38 mmol) were dissolved into 7.36 mL of DMF and 1.84 mL of MeOH. The mixture was heated at 180 °C during 50 h. The obtained pale brown powder was recovered by filtration and washed with DMF and MeOH and dried under air (~480 mg recovered).

For the solid prepared using acetic acid, the same procedure was followed, adding 0.286 mL of AcOH (5 mmol, H⁺/M ratio = 10) after the addition of the solvents.

Activation of MIL-47(V)-(SCH₃)₂: 200 mg of solid were suspended into 5 mL of MeOH under stirring. After 2 h, the solid was recovered by centrifugation and dried under air.

Crystallographic studies:

SC-XRD data from (DMA)KVO(DSBDC) were collected at room using a Rigaku XtaLAB Synergy diffractometer working at the Mo K α radiation. The CrysAlisPro suite was used to integrate and scale intensities and a semi-empirical absorption correction (ABSPACK) were applied on the basis of multiple scans of equivalent reflections. The structure was solved by using SHELXT⁵⁹ and refined with the full matrix least squares routine SHELXL⁶⁰. Non H-atoms were refined anisotropically. H atoms were placed in calculated positions and refined with idealized geometries.

MIL-47(V)-(SCH₃)₂ structure was elucidated from powder X-ray diffraction (PXRD) data collected on the CRISTAL beamline at Synchrotron SOLEIL (L'Orme des Merisiers, France). A monochromatic beam was extracted from the U20 undulator beam by means of a Si(111) double monochromator. Its wavelength of 0.671415 Å was refined from a LaB₆ (NIST Standard Reference Material 660a) powder diagram recorded prior to the experiment. The sample was loaded in a 0.7 mm capillary (Borokapillaren, GLAS, Schönwalde, Germany) mounted on a spinner rotating at about 5 Hz to improve the particles' statistics. Diffraction data were collected in continuous scanning mode with a MYTHEN2 X 9K detector (Dectris) allowing a measurement in less than 5 minutes. Calculations of structural investigations were performed with the TOPAS (indexing, simulated annealing, difference Fourier calculations and Rietveld refinement), and EXPO (whole powder pattern decomposition and Direct methods calculations) programs.^{59,60} The LSI-indexing method converged unambiguously to monoclinic unit cell with $M_{20} = 87$ (see Table 1). Systematic extinctions were consistent with the $C2/c$ space group, which was used to initialize the structural determination. Direct methods led us to locate the vanadium atom on a symmetry center. The organic ligand also localized on a symmetry center was then treated as rigid body, and its orientation was allowed to vary during a simulated annealing process. The guest DMF was located by both difference Fourier calculations and simulated annealing process. The final Rietveld plot (Figure S7), corresponds to satisfactory model indicator and profile factors (see Table S2). This involves 24 structural parameters: 1 scale factor, 1 atomic coordinate for the O3 atom, 9 parameters for the orientation and the translation of the organic moieties, 5 distances and 4 angles inside the organic ligand, 3 temperature factors and 1 occupancy factor for the DMF molecule.

CCDC-2246050, and CCDC-2497420 contain the supplementary crystallographic data for (DMA)KVO(DSBDC) and MIL-47(V)-(SCH₃)₂. These data can be obtained free of charge from the Cambridge Crystallographic Data Centre via <http://www.ccdc.cam.ac.uk/Community/Requestastructure>.



*Physicochemical characterizations:*View Article Online
DOI: 10.1039/D5QI02257F

PXRD patterns were collected either in a Bragg-Brentano mode with a Bruker D8 Advance diffractometer, or in a Debye-Scherrer mode with an INEL XRG3500 diffractometer, both equipped with a Cu anode ($\lambda = 1.5406 \text{ \AA}$).

Thermodiffraction experiments were carried out in an Anton Paar XRK 900 high-temperature chamber with the Bruker D8 Advance diffractometer. TGA were collected under Air at 5°C min^{-1} up to 800°C on a Setaram SENSYSevo equipment. For the ICP-AES experiments, solids were first dissolved in a 20% w/w HNO_3 and further analyzed thanks to an iCAP 6300 radial analyser (Thermo Scientific). Inductively coupled plasma mass spectrometry (ICP-MS) experiments were performed in a Perkin SCIEX NexION 300D at Servicios Centrales de Apoyo a la Investigación (SCAI), University of Málaga. Prior to the analysis, the samples were dehydrated and then digested in a HNO_3 solution (20% w/w) at 60°C . Elemental analyses were carried out in a Flash 2000 analyzer from Thermo Scientific. N_2 sorption experiments were carried out in a Micromeritics 3Flex equipment. The samples were degassed at 150°C during 16h under secondary vacuum prior to their analysis. Scanning electron microscopy (SEM) was carried out on a JEOL JSM-5800LV microscope. Samples were pasted on carbon tape and further coated with carbon to improve the surface electronic conductivity. Optical microscope images were acquired using a Zeiss SteREO Discovery V20 microscope equipped with a Zeiss Axiocam 208 color digital camera.

Fourier transformed infrared (FTIR) spectra were recorded at room temperature with a Bruker alpha FTIR spectrometer in the attenuated total reflectance (ATR) mode between 400 and 4000 cm^{-1} . Diffuse reflectance UV-Vis spectra were collected in a Perkin Elmer lambda 1050 equipped with an integration sphere modulus. Photoluminescence spectra were acquired in an FS5 fluorescence spectrophotometer (Edinburgh instruments) using a Xe lamp, exciting at 415 nm (4 slits).

Photocatalytic desulfurization experiments

The visible-light-driven ODS reactions were carried out in a 20 mL glass reactor. In a typical liquid-solid (L(ACN)-S(catalyst)) system experiment, 20 mg of photocatalyst, 10 mL of a 575 ppm DBT solution in ACN and 10 or 20 μL of a solution of 30% H_2O_2 (0.097 or 0.194 mmol) were added to the flask. The resulting dispersion was stirred at 900 rpm and exposed to visible light irradiation (using a 300 W Xe lamp at $\lambda > 400 \text{ nm}$). After 3 h, the photocatalyst was separated by centrifugation and the supernatant was analyzed using high-performance liquid chromatography (HPLC) (Jasco LC-4000 series system, equipped with a photodiode array detector (PDA) MD-4015, C18 column $5 \mu\text{m}$, $4.6 \times 250 \text{ mm}$). The mobile phase consisted of a mixture of 90:10 ACN: H_2O , with a flow rate of $0.8 \text{ mL} \cdot \text{min}^{-1}$.

For the liquid-liquid-solid (L(ACN)-L(oil)-S(catalyst)) system, the reaction was performed in a biphasic mixture composed of 10 mL of a 575 ppm DBT solution in n-octane and 5 mL of ACN as the extracting solvent, in the presence of 20 mg of photocatalyst and 20 or 40 μL of 30% H_2O_2 (0.194 mmol). The oil phase was analyzed by gas chromatography (GC) (Agilent GC 8860, equipped with a FID detector, HP-PLOT 5A column 30 m, 0.53 mm, 25 μm). The injector and detector temperatures were set to 290 and 310°C , respectively. The column temperature was maintained at 80°C for 1 min, then increased to 200°C at a ramp rate of $15^\circ\text{C min}^{-1}$ and held at 200°C for 10 min.

For recycling experiments, the photocatalyst was separated by centrifugation, washed with ACN and dried at 100°C for 2 h. Then, the photocatalyst was placed in contact with a fresh DBT solution under identical conditions.

Acknowledgements

Authors acknowledge the Agence Nationale de la Recherche for the funding of the project 'ThioMOFs' (grant ANR-19-CE08-0029-01 and -03) and NAPOLION project (PID2022-139956OB-I00) funded by MICIU/AEI /10.13039/501100011033 and by FEDER, UE. The synchrotron SOLEIL is thanked for providing access to the CRISTAL beamline, and Erik Elkaïm for the PXRD data collection. The ICP-AES analyses were performed at the LPG-UMR 6112 (C. La, M. Rivoal), Nantes Université, who is also thanked. P.S.-A. thanks Grant JDC2022-048964-I funded by MICIU/AEI/10.13039/501100011033 and by "European Union NextGenerationEU/PRTR". For the purpose of Open Access, a CC-BY public copyright licence has been applied by the authors to the present document and will be applied to all subsequent versions up to the Author Accepted Manuscript arising from this submission. Funding for open access charge: Universidad de Granada

References

- (1) New WHO Global Air Quality Guidelines aim to save millions of lives from air pollution. <https://www.who.int/news/item/22-09-2021-new-who-global-air-quality-guidelines-aim-to-save-millions-of-lives-from-air-pollution> (accessed 2025-09-04).
- (2) Orellano, P.; Reynoso, J.; Quaranta, N. Short-Term Exposure to Sulphur Dioxide (SO₂) and All-Cause and Respiratory Mortality: A Systematic Review and Meta-Analysis. *Environment International* **2021**, *150*, 106434. <https://doi.org/10.1016/j.envint.2021.106434>.
- (3) Saha, B.; Vedachalam, S.; Dalai, A. K. Review on Recent Advances in Adsorptive Desulfurization. *Fuel Processing Technology* **2021**, *214*, 106685. <https://doi.org/10.1016/j.fuproc.2020.106685>.
- (4) Haruna, A.; Merican, Z. M. A.; Musa, S. G. Recent Advances in Catalytic Oxidative Desulfurization of Fuel Oil – A Review. *Journal of Industrial and Engineering Chemistry* **2022**, *112*, 20–36. <https://doi.org/10.1016/j.jiec.2022.05.023>.
- (5) Peng, C.; Guo, R.; Feng, X.; Fang, X. Tailoring the Structure of Co-Mo/Mesoporous γ -Al₂O₃ Catalysts by Adding Multi-Hydroxyl Compound: A 3000 Kt/a Industrial-Scale Diesel Ultra-Deep Hydrodesulfurization Study. *Chemical Engineering Journal* **2019**, *377*, 119706. <https://doi.org/10.1016/j.cej.2018.08.092>.
- (6) Shafiq, I.; Shafique, S.; Akhter, P.; Ishaq, M.; Yang, W.; Hussain, M. Recent Breakthroughs in Deep Aerobic Oxidative Desulfurization of Petroleum Refinery Products. *Journal of Cleaner Production* **2021**, *294*, 125731. <https://doi.org/10.1016/j.jclepro.2020.125731>.
- (7) Wang, C.; Li, A.-R.; Ma, Y.-L. Phosphomolybdic Acid Nixed in the Metal-Organic Framework UiO-66 with Defects: An Efficient and Stable Catalyst for Oxidative Desulfurization. *Fuel Processing Technology* **2021**, *212*, 106629. <https://doi.org/10.1016/j.fuproc.2020.106629>.
- (8) Raeisi, A.; Najafi Chermahini, A.; Momeni, M. M. A Novel Photocatalytic and Photoelectrocatalytic System for Oxidative Desulfurization of Model Fuel Using BiVO₄@HKUST-1 Composite in Powder and Deposited on Fluorine-Doped Tin Oxide. *Journal of Photochemistry and Photobiology A: Chemistry* **2022**, *433*, 114190. <https://doi.org/10.1016/j.jphotochem.2022.114190>.
- (9) Salehian, S.; Larimi, A.; Asgharinezhad, A. A.; Khallaghi, N.; Borhani, T. N.; Ghotbi, C. Magnetic Z-Scheme Bismuth Molybdate(1-x)/Fe₃O₄@MIL-125(Ti)(x) Nanocomposite as a High-Performance Visible-Light-Active Photocatalyst for Ultra-Deep Oxidative Desulfurization of Liquid Fuel. *Surfaces and Interfaces* **2023**, *42*, 103432. <https://doi.org/10.1016/j.surfin.2023.103432>.



- (10) Beshtar, M.; Larimi, A.; Asgharinezhad, A. A.; Khorasheh, F. Ultra-Deep Photocatalytic Oxidative Desulfurization of Model Fuel Using Ti-Uio-66(Zr) Metal–Organic Framework. *Catal Lett* **2024**, *154* (6), 2633–2647. <https://doi.org/10.1007/s10562-023-04506-9>. View Article Online
DOI: 10.1039/D5QI02257F
- (11) Flihh, S. M.; Ammar, S. H. Zeolitic Imidazolate Framework Grafted by Cobalt Tungstate as an Efficient Photocatalyst for Photocatalytic Oxidative Desulfurization of Dibenzothiophene. *Materials Science in Semiconductor Processing* **2022**, *149*, 106894. <https://doi.org/10.1016/j.mssp.2022.106894>.
- (12) Fakhri, H.; Esrafil, A.; Farzadkia, M.; Boukherroub, R.; Srivastava, V.; Sillanpää, M. Preparation of Tungstophosphoric Acid/Cerium-Doped NH₂-UiO-66 Z-Scheme Photocatalyst: A New Candidate for Green Photo-Oxidation of Dibenzothiophene and Quinoline Using Molecular Oxygen as the Oxidant. *New Journal of Chemistry* **2021**, *45* (24), 10897–10906. <https://doi.org/10.1039/D1NJ00328C>.
- (13) Zhang, K.; Chu, F.; Hu, Y.; Huang, X.; Zhao, G.; Wang, G. Ce-Doped MIL-125-NH₂ Coupled Ce⁴⁺/Ce³⁺ and Ti⁴⁺/Ti³⁺ Redox Mediators for Thermo-Enhanced Photocatalytic Oxidative Desulfurization. *Chinese Chemical Letters* **2023**, *34* (5), 107766. <https://doi.org/10.1016/j.ccl.2022.107766>.
- (14) Alhaddad, M.; Shawky, A.; Zaki, Z. I. Photocatalytic Oxidative Desulfurization of Thiophene by Exploiting a Mesoporous V₂O₅-ZnO Nanocomposite as an Effective Photocatalyst. *Catalysts* **2022**, *12* (9), 933. <https://doi.org/10.3390/catal12090933>.
- (15) Belousov, A. S.; Shafiq, I. Towards the Sustainable Production of Ultra-Low-Sulfur Fuels through Photocatalytic Oxidation. *Catalysts* **2022**, *12* (9), 1036. <https://doi.org/10.3390/catal12091036>.
- (16) Pan, Y.; Sanati, S.; Abazari, R.; Jankowska, A.; Goscińska, J.; Srivastava, V.; Lassi, U.; Gao, J. Vanadium- and Manganese-Based Metal-Organic Frameworks for Potential Environmental and Catalysis Applications. *Coordination Chemistry Reviews* **2025**, *522*, 216231. <https://doi.org/10.1016/j.ccr.2024.216231>.
- (17) Pearson, R. G. Hard and Soft Acids and Bases. *Journal of the American Chemical Society* **1963**, *85* (22), 3533–3539. <https://doi.org/10.1021/ja00905a001>.
- (18) Sun, L.; Miyakai, T.; Seki, S.; Dincă, M. Mn₂ (2,5-Disulfhydrylbenzene-1,4-Dicarboxylate): A Microporous Metal–Organic Framework with Infinite (–Mn–S–) ∞ Chains and High Intrinsic Charge Mobility. *Journal of the American Chemical Society* **2013**, *135* (22), 8185–8188. <https://doi.org/10.1021/ja4037516>.
- (19) Sun, L.; Hendon, C. H.; Minier, M. A.; Walsh, A.; Dincă, M. Million-Fold Electrical Conductivity Enhancement in Fe₂ (DEBDC) versus Mn₂ (DEBDC) (E = S, O). *Journal of the American Chemical Society* **2015**, *137* (19), 6164–6167. <https://doi.org/10.1021/jacs.5b02897>.
- (20) He, J.; Yang, C.; Xu, Z.; Zeller, M.; Hunter, A. D.; Lin, J. Building Thiol and Metal-Thiolate Functions into Coordination Nets: Clues from a Simple Molecule. *Journal of Solid State Chemistry* **2009**, *182* (7), 1821–1826. <https://doi.org/10.1016/j.jssc.2009.04.024>.
- (21) Du, S.; Cui, M.; He, Z. Approach toward Iron(II) Coordination Polymers Based on Chain Motifs with Thiolate or Mixed Thiolate/Carboxylate Bridges: Structures and Magnetic Properties. *Inorganic Chemistry* **2021**, *60* (24), 19053–19061. <https://doi.org/10.1021/acs.inorgchem.1c02905>.
- (22) He, J.; Ye, X.; Liu, Z.; Tang, L.; Hu, J.; Xu, Z. Telltale Diamagnetism at 50 K of a Coordination Polymer System. *Materials Research Letters* **2022**, *10* (7), 496–500. <https://doi.org/10.1080/21663831.2022.2057822>.



- (23) Yee, K. K.; Reimer, N.; Liu, J.; Cheng, S. Y.; Yiu, S. M.; Weber, J.; Stock, N.; Xu, Z. Effective Mercury Sorption by Thiol-Laced Metal-Organic Frameworks: In Strong Acid and the Vapor Phase. *Journal of the American Chemical Society* **2013**, *135* (21), 7795–7798. https://doi.org/10.1021/JA400212K/SUPPL_FILE/JA400212K_SI_001.PDF. Article Online
DOI: 10.1039/D5QI02257F
- (24) Munn, A. S.; Millange, F.; Frigoli, M.; Guillou, N.; Falaise, C.; Stevenson, V.; Volkringer, C.; Loiseau, T.; Cibir, G.; Walton, R. I. Iodine Sequestration by Thiol-Modified MIL-53(Al). *CrystEngComm* **2016**, *18* (41), 8108–8114. <https://doi.org/10.1039/C6CE01842D>.
- (25) Li, M.-Q.; Wong, Y.-L.; Lum, T.-S.; Sze-Yin Leung, K.; Lam, P. K. S.; Xu, Z. Dense Thiol Arrays for Metal–Organic Frameworks: Boiling Water Stability, Hg Removal beyond 2 Ppb and Facile Crosslinking. *Journal of Materials Chemistry A* **2018**, *6* (30), 14566–14570. <https://doi.org/10.1039/C8TA04020F>.
- (26) Wong, Y.-L.; Diao, Y.; He, J.; Zeller, M.; Xu, Z. A Thiol-Functionalized UiO-67-Type Porous Single Crystal: Filling in the Synthetic Gap. *Inorganic Chemistry* **2019**, *58* (2), 1462–1468. <https://doi.org/10.1021/acs.inorgchem.8b03000>.
- (27) Cheng, S.; Ouyang, J.; Li, M.; Diao, Y.; Yao, J.; Li, F.; Lee, Y.; SUNG, H. H.; Williams, I.; Xu, Z.; Quan, Y. Charge Separation in Metal-Organic Framework Enables Heterogeneous Thiol Catalysis. *Angewandte Chemie International Edition* **2023**, *62* (25), e202300993. <https://doi.org/10.1002/anie.202300993>.
- (28) Chen, T.-F.; Han, S.-Y.; Wang, Z.-P.; Gao, H.; Wang, L.-Y.; Deng, Y.-H.; Wan, C.-Q.; Tian, Y.; Wang, Q.; Wang, G.; Li, G.-S. Modified UiO-66 Frameworks with Methylthio, Thiol and Sulfonic Acid Function Groups: The Structure and Visible-Light-Driven Photocatalytic Property Study. *Applied Catalysis B: Environmental* **2019**, *259*, 118047. <https://doi.org/10.1016/j.apcatb.2019.118047>.
- (29) Gedikoglu, N.; Salcedo-Abraira, P.; Nguyen, L. H. B.; Guillou, N.; Dupré, N.; Payen, C.; Louvain, N.; Stievano, L.; Poizot, P.; Devic, T. Fe(μ_3 -O)-Carboxythiolate Layered Metal–Organic Frameworks with Interest as Active Materials for Rechargeable Alkali-Ion Batteries. *Journal of Materials Chemistry A* **2023**, *11* (44), 23909–23921. <https://doi.org/10.1039/D3TA05353A>.
- (30) Nguyen, L. H. B.; Salcedo-Abraira, P.; Le Thanh, D.; Gedikoglu, N.; Guillou, N.; Coatleven, R.; Poizot, P.; Salles, F.; Louvain, N.; Stievano, L.; Devic, T. A Fe-Thiolate Layered Metal Organic Framework as a High-Performance Electrode Material for Potassium-Ion Batteries. *Chemical Communications* **2025**, *61* (53), 9614–9617. <https://doi.org/10.1039/D5CC02470F>.
- (31) Vial, L.; Ludlow, R. F.; Leclaire, J.; Pérez-Fernandez, R.; Otto, S. Controlling the Biological Effects of Spermine Using a Synthetic Receptor. *Journal of the American Chemical Society* **2006**, *128* (31), 10253–10257. <https://doi.org/10.1021/ja062536b>.
- (32) Stock, N. High-Throughput Investigations Employing Solvothermal Syntheses. *Microporous and Mesoporous Materials* **2010**, *129* (3), 287–295. <https://doi.org/10.1016/j.micromeso.2009.06.007>.
- (33) Barthelet, K.; Marrot, J.; Férey, G.; Riou, D. VIII(OH){O₂C–C₆H₄–CO₂}.(HO₂C–C₆H₄–CO₂H)_x(DMF)_y(H₂O)_z (or MIL-68), a New Vanadocarboxylate with a Large Pore Hybrid Topology: Reticular Synthesis with Infinite Inorganic Building Blocks? *Chemical Communications* **2004**, *4* (5), 520–521. <https://doi.org/10.1039/B312589K>.
- (34) Lu, Z.; Godfrey, H. G. W.; da Silva, I.; Cheng, Y.; Savage, M.; Manuel, P.; Rudić, S.; Ramirez-Cuesta, A. J.; Yang, S.; Schröder, M. Direct Observation of Supramolecular Binding of Light Hydrocarbons in Vanadium(μ_3 -O) and (μ_3 -O) Metal–Organic Framework Materials. *Chemical Science* **2018**, *9* (13), 3401–3408. <https://doi.org/10.1039/C8SC00330K>.



- (35) Barthelet, K.; Adil, K.; Millange, F.; Serre, C.; Riou, D.; Férey, G. Synthesis, Structure Determination and Magnetic Behaviour of the First Porous Hybrid Oxyfluorinated Vanadocarboxylate: MIL-71 or $V^{III}_2(OH)_2F_2(O_2C-C_6H_4)_2$. *J. Mater. Chem.* **2003**, 13 (9), 2208–2212. <https://doi.org/10.1039/B306852H>. View Article Online
DOI: 10.1039/B306852H
- (36) Barthelet, K.; Marrot, J.; Riou, D.; Férey, G. A Breathing Hybrid Organic–Inorganic Solid with Very Large Pores and High Magnetic Characteristics. *Angewandte Chemie International Edition* **2002**, 41 (2), 281. [https://doi.org/10.1002/1521-3773\(20020118\)41:2<281::AID-ANIE281>3.0.CO;2-Y](https://doi.org/10.1002/1521-3773(20020118)41:2<281::AID-ANIE281>3.0.CO;2-Y).
- (37) Barthelet, K.; Riou, D.; Férey, G. [VIII(H₂O)]₃O(O₂CC₆H₄CO₂)₃·(Cl, 9H₂O) (MIL-59): A Rare Example of Vanadocarboxylate with a Magnetically Frustrated Three-Dimensional Hybrid Framework. *Chemical Communications* **2002**, 2 (14), 1492–1493. <https://doi.org/10.1039/B202749F>.
- (38) Carson, F.; Su, J.; Platero-Prats, A. E.; Wan, W.; Yun, Y.; Samain, L.; Zou, X. Framework Isomerism in Vanadium Metal–Organic Frameworks: MIL-88B(V) and MIL-101(V). *Crystal Growth & Design* **2013**, 13 (11), 5036–5044. <https://doi.org/10.1021/cg4012058>.
- (39) Biswas, S.; Couck, S.; Grzywa, M.; Denayer, J. F. M.; Volkmer, D.; Van Der Voort, P. Vanadium Analogues of Nonfunctionalized and Amino-Functionalized MOFs with MIL-101 Topology – Synthesis, Characterization, and Gas Sorption Properties. *European Journal of Inorganic Chemistry* **2012**, 2012 (15), 2481–2486. <https://doi.org/10.1002/ejic.201200106>.
- (40) Lieb, A.; Leclerc, H.; Devic, T.; Serre, C.; Margiolaki, I.; Mahjoubi, F.; Lee, J. S.; Vimont, A.; Daturi, M.; Chang, J.-S. MIL-100(V) – A Mesoporous Vanadium Metal Organic Framework with Accessible Metal Sites. *Microporous and Mesoporous Materials* **2012**, 157, 18–23. <https://doi.org/10.1016/j.micromeso.2011.12.001>.
- (41) Barthelet, K.; Riou, D.; Nogues, M.; Férey, G. Synthesis, Structure, and Magnetic Properties of Two New Vanadocarboxylates with Three-Dimensional Hybrid Frameworks. *Inorganic Chemistry* **2003**, 42 (5), 1739–1743. <https://doi.org/10.1021/ic026175m>.
- (42) Liu, Y.; Leus, K.; Grzywa, M.; Weinberger, D.; Strubbe, K.; Vrielinck, H.; Van Deun, R.; Volkmer, D.; Van Speybroeck, V.; Van Der Voort, P. Synthesis, Structural Characterization, and Catalytic Performance of a Vanadium-Based Metal–Organic Framework (COMOC-3). *European Journal of Inorganic Chemistry* **2012**, 2012 (16), 2819–2827. <https://doi.org/10.1002/ejic.201101099>.
- (43) Zhang, Z.; Zaworotko, M. J. Template-Directed Synthesis of Metal–Organic Materials. *Chem. Soc. Rev.* **2014**, 43 (16), 5444–5455. <https://doi.org/10.1039/C4CS00075G>.
- (44) Richards, R. L. Vanadium: Inorganic & Coordination Chemistry Based in Part on the Article Vanadium: Inorganic & Coordination Chemistry by Elizabeth M. Page & Sherilyn A. Wass Which Appeared in the Encyclopedia of Inorganic Chemistry, First Edition. In *Encyclopedia of Inorganic and Bioinorganic Chemistry*; John Wiley & Sons, Ltd: Chichester, UK, 2011. <https://doi.org/10.1002/9781119951438.eibc0236>.
- (45) Mkhadder, H.; Denis, M.; Giménez-Marqués, M.; Cañón-Mancisidor, W.; Humbert, B.; Deunf, E.; Poizot, P.; Devic, T. A Tris-Oxovanadium Pyrogallate Complex: Synthesis, Structure, and Magnetic and Electronic Properties. *Dalton Transactions* **2021**, 50 (38), 13399–13406. <https://doi.org/10.1039/D1DT01990B>.
- (46) Brese, N. E.; O’Keeffe, M. Bond-Valence Parameters for Solids. *Acta Crystallographica Section B Structural Science* **1991**, 47 (2), 192–197. <https://doi.org/10.1107/S0108768190011041>.



- (47) Leclerc, H.; Devic, T.; Devautour-Vinot, S.; Bazin, P.; Audebrand, N.; Férey, G.; Daturi, M.; Vimont, A.; Clet, G. Influence of the Oxidation State of the Metal Center on the Flexibility and Adsorption Properties of a Porous Metal Organic Framework: MIL-47(V). *The Journal of Physical Chemistry C* **2011**, *115* (40), 19828–19840. <https://doi.org/10.1021/jp206655y>. View Article Online
DOI: 10.1039/D5QI02257F
- (48) Bashkin, J. S.; Huffman, J. C.; Christou, G. A Synthetic Model Approach to the Manganese(III) Acid Phosphatase and Its Iron(III)-Substituted Form. *Journal of the American Chemical Society* **1986**, *108* (16), 5038–5039. <https://doi.org/10.1021/ja00276a072>.
- (49) Duran, N.; Clegg, W.; Cucurull-Sánchez, L.; Coxall, R. A.; Jiménez, H. R.; Moratal, J.-M.; Lloret, F.; González-Duarte, P. Unprecedented Stabilization of Cobalt(II) in a Tetrahedral S₂O₂ Environment: The Use of a Redox-Noninnocent Ligand. *Inorganic Chemistry* **2000**, *39* (21), 4821–4832. <https://doi.org/10.1021/ic000223q>.
- (50) Karet, G. B.; Castro, S. L.; Folting, K.; Bollinger, J. C.; Heintz, R. A.; Christou, G. Dinuclear, Trinuclear and Mixed-Metal Hexanuclear Aggregates of Vanadium: Crystal Structures and Properties of [NEt₄]₃[V₂Cl₉], [PPh₄]₂[V₃OCl₄(O₂CC₆H₄SH)₅] and [NEt₄]₄[V₂Li₄O₂Cl₄(O₂CC₆H₄S)₄]⁺. *Journal of the Chemical Society, Dalton Transactions* **1998**, No. 1, 67–72. <https://doi.org/10.1039/a705752k>.
- (51) Hegetschweiler, K.; Keller, T.; Baeumle, M.; Rihs, G.; Schneider, W. Electrochemical Reduction of Complexes Containing the [Mo₃S(S₂)₃]⁴⁺ Core in Aqueous Media and the Structure of Bis(Triethylammonium) Tris(2-Mercaptobenzoato)Tris(μ-Disulfido)(μ₃-Thio)-Triangulo-Trimolybdate(IV). *Inorganic Chemistry* **1991**, *30* (23), 4342–4347. <https://doi.org/10.1021/ic00023a011>.
- (52) Serre, C.; Millange, F.; Devic, T.; Audebrand, N.; Van Beek, W. Synthesis and Structure Determination of New Open-Framework Chromium Carboxylate MIL-105 or CrIII(OH)·{O₂C–C₆(CH₃)₄–CO₂}·nH₂O. *Materials Research Bulletin* **2006**, *41* (8), 1550–1557. <https://doi.org/10.1016/j.materresbull.2006.01.013>.
- (53) Devic, T.; Horcajada, P.; Serre, C.; Salles, F.; Maurin, G.; Moulin, B.; Heurtaux, D.; Clet, G.; Vimont, A.; Grenèche, J.-M.; Ouay, B. Le; Moreau, F.; Magnier, E.; Filinchuk, Y.; Marrot, J.; Lavalley, J.-C.; Daturi, M.; Férey, G. Functionalization in Flexible Porous Solids: Effects on the Pore Opening and the Host–Guest Interactions. *Journal of the American Chemical Society* **2010**, *132* (3), 1127–1136. <https://doi.org/10.1021/ja9092715>.
- (54) Li, X.; Gu, Y.; Chu, H.; Ye, G.; Zhou, W.; Xu, W.; Sun, Y. MFM-300(V) as an Active Heterogeneous Catalyst for Deep Desulfurization of Fuel Oil by Aerobic Oxidation. *Applied Catalysis A: General* **2019**, *584*, 117152. <https://doi.org/10.1016/j.apcata.2019.117152>.
- (55) Ahmed, I.; Kim, C.-U.; Jhung, S. H. Carbon-Supported Vanadium Nitride Catalyst, Prepared from Urea-Loaded MIL-100(V) in the Absence of External Ammonia Flow, Having Good Performance in Oxidative Desulfurization. *Journal of Cleaner Production* **2023**, *384*, 135509. <https://doi.org/10.1016/j.jclepro.2022.135509>.
- (56) McNamara, N. D.; Neumann, G. T.; Masko, E. T.; Urban, J. A.; Hicks, J. C. Catalytic Performance and Stability of (V) MIL-47 and (Ti) MIL-125 in the Oxidative Desulfurization of Heterocyclic Aromatic Sulfur Compounds. *Journal of Catalysis* **2013**, *305*, 217–226. <https://doi.org/10.1016/j.jcat.2013.05.021>.
- (57) Huo, Q.; Liu, G.; Sun, H.; Fu, Y.; Ning, Y.; Zhang, B.; Zhang, X.; Gao, J.; Miao, J.; Zhang, X.; Liu, S. CeO₂-Modified MIL-101(Fe) for Photocatalysis Extraction Oxidation Desulfurization of Model Oil under



Visible Light Irradiation. *Chemical Engineering Journal* **2021**, *422*, 130036. <https://doi.org/10.1016/j.cej.2021.130036>. Article Online
DOI: 10.1039/D5QI02257F

(58) Smolders, S.; Willhammar, T.; Krajnc, A.; Sentosun, K.; Wharmby, M. T.; Lomachenko, K. A.; Bals, S.; Mali, G.; Roeffaers, M. B. J.; De Vos, D. E.; Bueken, B. A Titanium(IV)-Based Metal–Organic Framework Featuring Defect-Rich Ti-O Sheets as an Oxidative Desulfurization Catalyst. *Angewandte Chemie International Edition* **2019**, *58* (27), 9160–9165. <https://doi.org/10.1002/anie.201904347>.

(59) Sheldrick, G. M. SHELXT – Integrated Space-Group and Crystal-Structure Determination. *Acta Crystallographica Section A Foundations and Advances* **2015**, *71* (1), 3–8. <https://doi.org/10.1107/S2053273314026370>.

(60) Sheldrick, G. M. Crystal Structure Refinement with SHELXL. *Acta Crystallographica Section C Structural Chemistry* **2015**, *71* (1), 3–8. <https://doi.org/10.1107/S2053229614024218>.



The data that support the findings of this study are available from the corresponding authors, Pablo Salcedo-Abraira, Yolanda Perez and Thomas Devic, upon reasonable request.

Full Article Online
DOI: 10.1039/D5QI02257F

